ELSEVIER

Contents lists available at ScienceDirect

Journal of Non-Crystalline Solids

journal homepage: www.elsevier.com/locate/jnoncrysol





Corrosion resistance enhancement of bulk metallic glass through ultrasonic vibrations

Lixing Zhu ^a, Luyao Li ^a, Jinbiao Huang ^a, Heting Zhang ^a, Wenxue Wang ^a, Jianyu Chen ^a, Junsheng Liu ^a, Jiang Ma ^{a,b,*}

- a Guangdong Provincial Key Laboratory of Micro/Nano Optomechatronics Engineering, Shenzhen University, Shenzhen, 518060, China
- b Shenzhen Key Laboratory of High Performance Nontraditional Manufacturing, College of Mechatronics and Control Engineering, Shenzhen University, Shenzhen, 518060. China

ARTICLE INFO

Keywords: Bulk metallic glass Ultrasonic vibrations Corrosion resistance Enhancement

ABSTRACT

Bulk metallic glass (BMG) possesses a range of desirable properties, including exceptional mechanical, soft magnetic, and catalytic properties, etc. However, to pursuit extensive specific applications, enhancing the corrosion resistance of BMG is required. Herein, an effective method involving ultrasonic vibrations (UV) treatment was proposed to significantly enhance the corrosion resistance of BMG. The self-corrosion potential of UV processed BMG increased by up to 0.14 V in 1 N HCl solution and 0.2 V in 3.5 % NaCl solution, respectively. Additionally, the maximum reduction in corrosion current density for the UV processed BMG in these solutions was 15 % and 20 %, respectively. Micro-morphology results indicated that the UV processed BMG exhibited better pitting resistance. It is found that a denser arrangement of BMG was obtained after UV which resulted in reduced relaxation enthalpy and enhanced corrosion resistance. This work introduces an innovative and convenient method to enhance the corrosion resistance of BMG for engineering applications.

1. Introduction

Corrosion refers to the chemical or electrochemical interaction between materials and the environment [1]. It can rapidly lead to materials failure during usage, thereby affecting their lifespan and strength [2]. Even worse, corrosion leads to significant resource wastage and economic losses, posing a great threat to the safety of national economies and property worldwide [3,4]. Therefore, to develop corrosion modification technology holds great social, economic, and practical significance.

Amorphous alloys, also known as metallic glasses, are a type of alloy that lacks long-range periodic crystal structure and translational symmetry. Due to their unique mechanical, physical, and chemical properties, bulk metallic glasses (BMGs) have attracted significant attention since their discovery [5-12]. BMGs exhibit outstanding properties compared to traditional crystalline materials, such as superior strength, excellent wear resistance and corrosion resistance [13-18], rendering them highly promising for applications in both fundamental science and industrial fields. In the past several decades, various types of corrosion-resistant BMGs have been developed [19]. The excellent

corrosion resistance of BMGs is not only influenced by alloying elements but also closely related to their metastable amorphous structure. Owing to the lack of grain boundaries, dislocations, stacking faults, and secondary phase precipitations, the propensity for preferential corrosion of BMGs can be relatively diminished [20-22].

To further broaden their application scope and attain superior corrosion resistance, a range of corrosion performance modification methods based on BMGs have emerged. Microalloying with specific elements is a common method used to enhance the corrosion resistance of BMGs, but it may potentially reduce the glass forming ability of the system [23,24]. In recent years, ion implantation technology [25] has been applied to enhance the corrosion resistance of BMGs, but it can introduce new elements that may affect other properties. Heat treatment methods [26] can also be employed to improve the corrosion resistance of BMGs, but the heat treatment process is inconvenient and time-consuming that sometimes may span hours or more [27]. The above methods for enhancing the corrosion resistance of BMGs are time-consuming, involve complex processing, and incur high costs. Therefore, there is an urgent need for a simple, convenient, and cost-effective method to enhance the corrosion resistance of BMGs.

E-mail address: majiang@szu.edu.cn (J. Ma).

^{*} Corresponding author.

Recently, ultrasonic vibrations (UV) technology has been successfully applied to the manufacturing of BMGs [28], including welding [29, 30] and molding [31], among other processes. In addition, it has been proved to be a fast and simple method to achieve structural modification of MGs, such as rejuvenation or relaxation, which could greatly affect the properties of them [30,32,33]. Here, we report a method to enhance the corrosion resistance of BMG through UV treatment. Through comparing the electrochemical parameters of the as-cast and UV processed samples, we found that the UV processed samples exhibited a higher self-corrosion potential and lower corrosion current density, which are important sign of enhanced corrosion resistance. Meanwhile, micro-morphological analysis revealed that the UV processed samples exhibited enhanced resistance to pitting corrosion. The results demonstrate that UV treatment significantly enhances the corrosion resistance of BMG in less than 1 s by swiftly making its atomic structure more tightly aligned and reducing relaxation enthalpy. It is expected that this work can provide new strategies and ideas to further enhance the corrosion resistance of BMGs.

2. Materials and methods

The alloy ingots with nominal composition of $\rm Zr_{55}Cu_{30}Ni_5Al_{10}$ with a mixture of elements with a purity of at least 99.9 % were prepared by arc melting method under a Ti-gettered high-purity argon atmosphere. Each ingot was remelted at least five times to make sure the chemical homogeneity of the composition. Cylindrical sample rods with diameter of 5 mm and length of 40 mm were prepared using copper mold suction casting. The sample rods were cut into multiple disks with thickness of 1.5 mm by a low-speed diamond cutting machine. The surfaces of the upper and lower ends were polished to maintain parallel.

Subsequently, the polished samples were subjected to UV treatment. The specific parameters of the UV equipment include welding pressure, input energy, etc. In this work, a UV frequency of 20,000 Hz was used. The UV process begins by placing the polished samples into a designated mold, followed by preloading with a low load of 22 N to ensure close contact between the sonotrode and sample. Upon contact, UV is released based on the input energy. Generally, this process only lasts a few seconds, depending on the magnitude of the input energy. In this work, energy inputs of 300 J and 600 J were used to apply UV. To obtain thermal effect during the UV process, an infrared thermal imaging camera with high accuracy of 1 K was utilized to monitor real-time temperature changes. Simultaneously, a precise force measuring instrument was used to monitor real-time changes in force throughout the UV process. In order to further investigate the phase structural changes of the samples before and after UV treatment, the X-ray diffraction (XRD, Rigaku MiniFlex 600) with Cu kα radiation was employed. The thermal response of the samples was confirmed by differential scanning calorimetry (DSC, Perkin-Elmer DSC-8000) a heating rate of 20 K/min, to measure the activation energy of the crystallization process. The transmission electron microscopy (TEM) samples were prepared on a FEI Scios SEM/FIB dual beam system at room temperature. The microstructure of the samples was characterized using TEM (TEM, FEI Titan Cubed Themis G2 300), and selected area electron diffraction (SAED) was performed under TEM mode.

The electrochemical tests were conducted by a CHI660e electrochemical workstation. In a three-electrode cell, the samples served as the working electrode, an Ag/AgCl electrode functioned as the reference electrode, and a platinum foil was employed as the counter electrode. Prior to the electrochemical tests, both as-cast and UV processed samples were mechanically polished to a mirror finish by 4000-grit size metallographic sandpaper, followed by degreasing in acetone, rinsing with alcohol and distilled water, and drying in air for 24 h. In this study, the electrolytes used were 1 N HCl and 3.5 % NaCl solution. To stabilize the open circuit potential, the samples were immersed for 30 min in the solutions, and then the polarization behavior of the samples were measured at a scan rate of 1 mV/s. Some samples were removed after

polarization to the pitting potential and subjected to morphological analysis by scanning electron microscopy (SEM, FEI QUANTA FEG 450). The corrosion behavior was comprehensively evaluated through electrochemical tests and morphological analysis of the samples after tests.

3. Results and discussion

The schematic diagram of the UV process and the overall morphology of both the as-cast and UV processed samples are depicted in Fig. 1a. We can see that the UV equipment comprises three main components: a transducer converting electrical energy into mechanical vibrations, a booster amplifying the vibrations amplitude, and a sonotrode transmitting the mechanical vibrations to the sample. Furthermore, the UV processed sample remain intact following the polishing treatment. Due to the UV lasts less than 1 s, there may be some thermal effects involved on the samples. Fig. 1b shows the temperature variation during the whole UV process. It can be found that the maximum temperature of the entire UV process is 411 K, which is still lower than their glass transition temperature (T_g) and returns to near room temperature after 2 s, effectively avoiding the influence of excessive temperature on the performance of the samples. As shown in Fig. 1c, when UV is operated, only a pressure of 14.37 MPa and a very short time of 0.14 s are required. Therefore, the UV process is a low temperature rise and low pressure process [34,35].

Fig. 1d shows the XRD patterns of the as-cast and UV processed samples. The patterns display only a broad diffraction peak without any obvious crystalline peaks, indicating that all samples are the completely amorphous state. To further confirm that the as-cast and UV processed samples do not contain crystallization, we compared the DSC traces of all samples at a heating rate of 20 K/min. The distinct glass transition signals and sharp crystalline peaks can be observed in Fig. 1e, indicating that the BMGs maintain an amorphous nature before and after UV treatment. The values of the glass transition temperature (T_g) , the onset temperature of crystallization (T_x), the resulting temperature interval of the supercooled liquid region ($\Delta T_x = T_x - T_g$), and the enthalpy for crystallization (H_{cryst}) are summarized in Table 1. It can be found that the values of T_g and T_x increase slightly after UV treatment, keeping the supercooled liquid region almost unchanged. The enthalpy for the crystallization of the UV processed samples shows a slight decrease with respect to the as-cast sample. This means that within a certain range of input energy, it has little effect on the thermal stability of the amorphous phase.

The electrochemical tests were designed to investigate the effect of UV treatment on the corrosion resistance of BMG. Fig. 2 shows the potentiodynamic behavior of the as-cast and UV processed samples in 1 N HCl and 3.5 % NaCl solutions open to air at room temperature. The electrochemical parameters of the samples including the open circuit potential (OCP), corrosion potential (E_{corr}), pitting potential (E_{pit}) and corrosion current density (I_{corr}) are summarized in Table 2. Performing OCP tests to stabilize the potential can effectively avoid the effect of large potential fluctuation on the results in electrochemical tests. As shown in Fig. 2a, The UV processed samples (300 J, -0.447 V; 600 J, −0.417 V) exhibit higher OCP values compared to the as-cast sample (-0.501 V), indicating reduced corrosion tendencies [36]. Fig. 2b shows the polarization curves of the as-cast and UV processed samples in 1 N HCl solution. It can be observed that all samples undergo active dissolution in 1 N HCl solution, and no self-passivation was observed in polarization curves. This is similar to the literatures, which suggest that Zr-based BMGs have poor corrosion resistance in HCl solution [37,38]. However, the UV processed samples exhibit the higher E_{corr} and E_{pit} and lower I_{corr} respect to the as-cast sample, demonstrating that the UV processed samples exhibits better corrosion resistance than the as-cast sample [39].

The result of corrosion tests in 3.5 % NaCl solution was different. The OCP values of all samples first fluctuated greatly and finally reached a relatively stable state, as shown in Fig. 2c, demonstrating that the

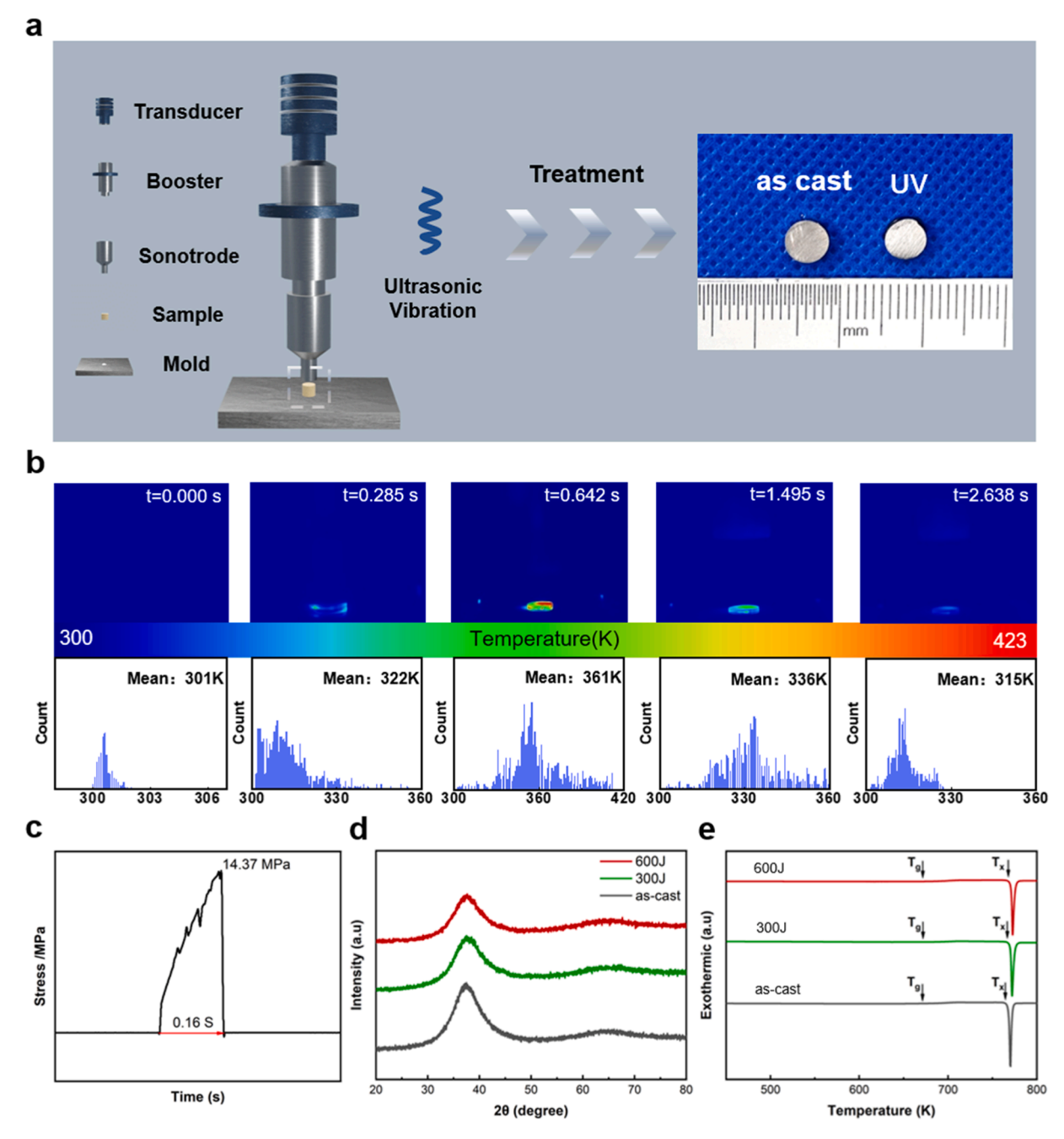


Fig. 1. (a) Schematic diagram of the UV equipment and the overall morphology of the as-cast and UV processed samples. (b) Temperature change during UV treatment for the sample with an input energy of 600 J. (c) The variation of UV stress with time under energy value of 600 J. (d) XRD patterns of as-cast and UV processed samples. (e) DSC curves of as-cast and UV processed samples, with arrows indicating T_g and T_x .

Table 1 Values of T_g , T_x , ΔT_x , and ΔH_{cryst} at a heating rate of 20 K/min.

	57 10 10	cryot		
Sample	$T_{\rm g}$ (K)	T_{x} (K)	ΔT_{x} (K)	$\Delta H_{\rm cryst}$ (J g ⁻¹)
as-cast	680	767	87	53.362
300J	681	768	87	51.527
600J	683	771	88	49.643

stability of passive film was enhanced during the immersion [40]. Similarly, the UV processed samples exhibit higher OCP than the as-cast sample. In Fig. 2d, we can see that the as-cast and UV processed samples were spontaneously passivated and show wide passivation areas with a similar $E_{\rm pit}$, ranging from $-0.30~{\rm V}$ to $-0.31~{\rm V}$. In addition, both $E_{\rm corr}$ and

 $I_{\rm corr}$ of the UV processed samples change significantly, showing higher $E_{\rm corr}$ and lower $I_{\rm corr}$, which indicates a reduced tendency to corrode [41, 42].

To further investigate the impact of UV treatment, we conducted electrochemical tests on both the flat surfaces and cross-sections of the samples. Some samples underwent UV treatment, as illustrated in Fig. 3a. Subsequently, the flat surfaces of both the as-cast and UV processed samples were subjected to identical duration of electrochemical tests in 1 N HCl solution. In Fig. 3(b and c), both samples exhibit typical corrosion pits of varying sizes and shapes, resulting from the rupture of the passive film. However, in the UV processed sample (see Fig. 3c), while some regions display corrosion pits, as shown in Fig. 3d, it is noteworthy that numerous areas with flat and less visibly ruptured passive films were found, as shown in Fig. 3e. Hence, the evidence from

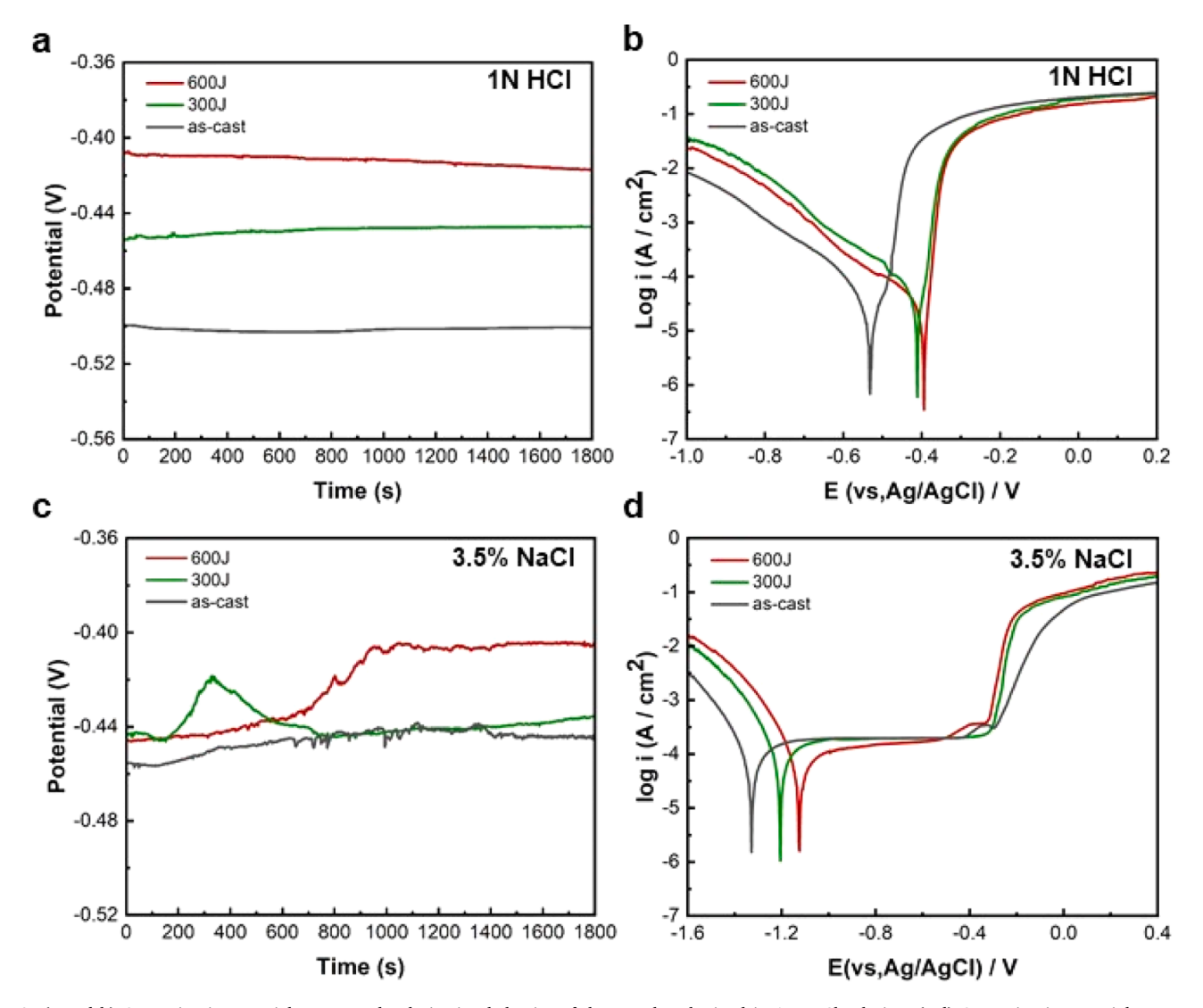


Fig. 2. (a and b) Open circuit potential curves and polarization behavior of the samples obtained in 1 N HCl solution. (c-d) Open circuit potential curves and polarization behavior of the samples obtained in 3.5 % NaCl solution.

Table 2 The electrochemical parameters (OCP, $E_{\rm corr}$, $E_{\rm pit}$, $I_{\rm corr}$) of the as-cast and UV processed samples.

Solution	Samples	OCP(V)	$E_{\rm corr}(V)$	$E_{\rm pit}(V)$	$I_{\rm corr}(10^{-5}{\rm A/cm}^2)$
1 N HCl	as-cast	-0.501	-0.532	-0.421	4.266
	300J	-0.447	-0.411	-0.329	3.891
	600J	-0.417	-0.394	-0.322	3.311
3.5 % NaCl	as-cast	-0.444	-1.329	-0.301	5.888
	300J	-0.436	-1.206	-0.307	5.012
	600J	-0.405	-1.124	-0.309	5.628

corrosion morphology suggests that UV treatment contributes to an enhancement in the corrosion resistance of the samples. To further confirm this result, we performed the same electrochemical tests on a cross-section of the UV processed sample, as shown in Fig. 3f. Interestingly, in Fig. 3g, we can observe that the pitting craters start growing from bottom to top, indicating that the areas farther from the UV treatment are the first to begin corrosion. Fig. 3h shows the corrosion morphology in the region exposed to UV, where the corrosion pits are barely visible. In contrast, Fig. 3i depicts the corrosion morphology in the region without UV exposure, where continuous growth of corrosion pits can be observed. Therefore, it can be inferred that UV treatment has

the potential to enhance the corrosion resistance of the BMG samples.

To visualize the differences in corrosion resistance of the both samples, Fig. 3(j-l) presents the corrosion morphology of the as-cast and UV processed samples after immersion in a 1 N HCl solution for 1, 3, and 5 days, respectively. It can be clearly observed that with increasing immersion time, the corrosion morphology of the as-cast sample becomes more complex. In addition, the number of pitting corrosion pits was greater in the as-cast sample and tended to expand compared to the UV processed sample.

We next study the corrosion mechanism of BMG after UV treatment. It has been proved that the chemical composition and amorphous structure have a significant influence on the corrosion behavior of BMG [18,25]. To exclude the effect of compositional changes on corrosion resistance, the elemental distributions of the samples were measured by the EDS under SEM. In Supplementary Fig. 1S, we can clearly see that the elemental content of the as-cast and UV processed samples was almost the same. This indicates that the enhancement of the corrosion resistance of the samples is not attributed to a change in chemical composition but is more likely due to alterations in the amorphous structure. To demonstrate that the enhancement in the corrosion resistance of the samples is indeed attributed to the change in its amorphous structure, TEM and DSC analyses of the samples were conducted.

Fig. 4(a and b) shows the high-resolution transmission electron

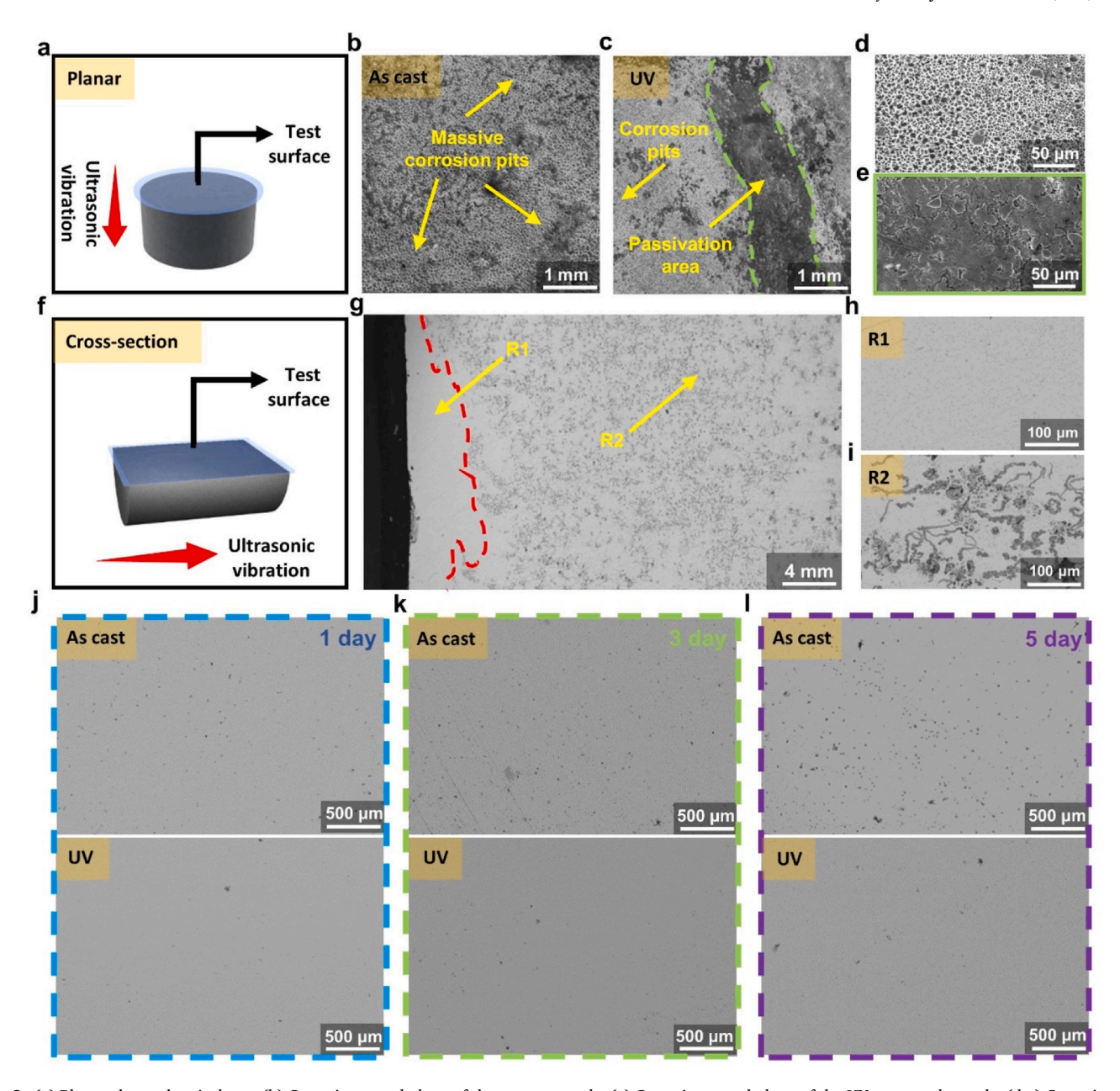


Fig. 3. (a) Planar electrochemical test. (b) Corrosion morphology of the as-cast sample. (c) Corrosion morphology of the UV processed sample. (d-e) Corrosion pits and passivation film area of the UV processed sample, respectively. (f) Cross-section electrochemical test. (g) Corrosion morphology of the UV processed sample's cross-section. (h) Corrosion morphology corresponding to the region exposed to UV. (i) Corrosion morphology corresponding to the region without UV exposure. (j-l) Comparison of corrosion morphology between the as-cast and UV processed samples immersed in 1 N HCl solution for 1, 3, and 5 days, respectively.

microscopy (HRTEM) images and the corresponding selective area diffraction patterns (SADPs) of the as-cast and UV processed samples, respectively. It is evident that both samples exhibit an amorphous state. Moreover, the radius of the SADP is observed to increase after UV treatment, as illustrates in Fig. 4c. Since the radius of the SADP is inversely proportional to the average atomic distance (D) in the region [43,44], we can determine the average atomic distance for both as cast and UV processed samples, thereby quantifying the change in free volume for the UV processed sample.

As shown inset in Fig. 4c, the as cast and UV processed samples have the following values of D: 2.74 and 2.69 Å, respectively. The third power of D is correlated with the mean atomic volume by equation [54]:

$$\frac{D_0^3}{D_{v_0}^2} = \frac{V_{UV}}{V_0} \tag{1}$$

where D_0 and D_{UV} is the average interatomic distance of as cast and UV processed samples, respectively; V_0 and V_{UV} is the mean atomic volume of as cast and UV processed samples, respectively. Relative changes in free volume could be estimated according to [55]:

$$\Delta V = \frac{D_{UV}^3 - D_0^3}{D_0^3} * 100\% \tag{2}$$

Thus, the free volume of the sample is reduced by 5.38 % after UV treatment. we infer that the amorphous structure of the UV processed samples undergoes alteration, with the atoms becoming denser.

To further verify that the UV processed samples undergo relaxation, the relaxation enthalpy values were measured by DSC curves to quantitatively determine the extent of BMG structural relaxation [45], as shown in Fig. 4d. It is worth noting that the broad specific heat exotherm preceding glass transition of the BMG is a characteristic of structural

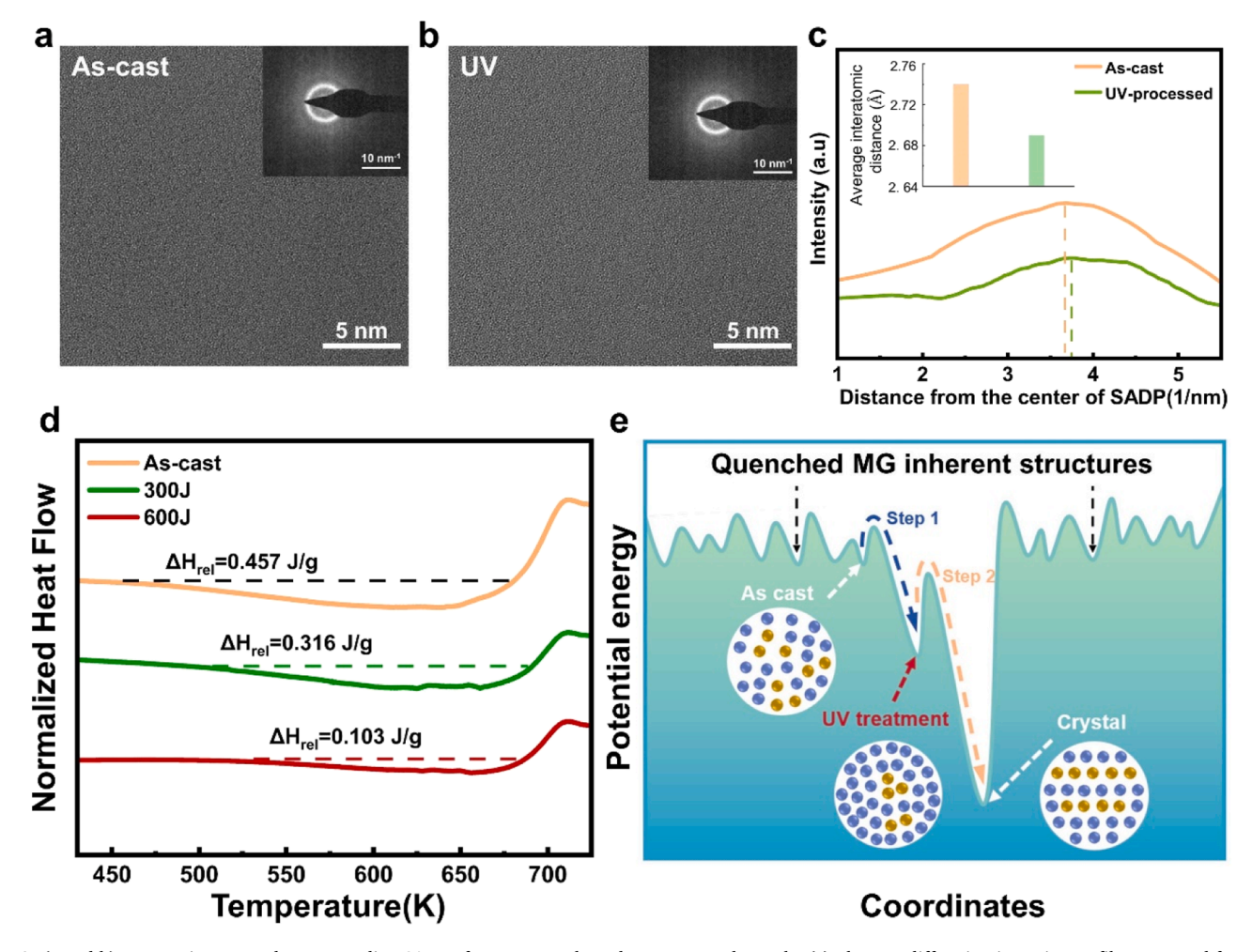


Fig. 4. (a and b) HRTEM images and corresponding SADP of as-cast sample and UV processed sample. (c) Electron diffraction intensity profiles extracted from the SADPs. Inset shows the corresponding average interatomic distance. (d) Relaxation exotherm of as-cast and UV processed samples. (e) Schematic diagram of the process of structural evolution and stabilization of the potential energy landscape under the action of UV.

relaxation [46]. The relaxation enthalpy values ($\Delta H_{\rm rel}$) of the as-cast and UV processed samples (300 J and 600 J) are 0.457 J/g, 0.316 J/g, and 0.103 J/g, respectively. We can see a significant reduction in the $\Delta H_{\rm rel}$ of the UV processed samples. The results demonstrate that UV treatment can rearrange the atoms inside the BMG, thus effectively eliminating some inelastic regions and excess free volume, etc. [47].

To investigate the process of amorphous structure evolution and stabilization of samples during UV treatment, we established a potential energy landscape as shown in Fig. 4e. We can see that the as-cast sample is quenched at a relatively high energy state, and after UV treatment, it can cross the energy barrier into the energy basin with lower potential energy and form a denser atomic stacking state. Due to the presence of a large number of inelastic regions with low activation energies in BMG [48,49], these inelastic regions are activated under high-frequency UV and form a denser arrangement. It has been reported that the corrosion behavior of BMG is closely related to the amorphous structure [50]. Moreover, UV treatment reduces the free volume of the BMG, consequently decreasing the average atomic distance and chemical potential. This benefits a more stable structure that enhances their corrosion resistance [50-52]. In contrast, excessive free volume and nano-vacancy can render BMG susceptible to chemical attack [53], consequently reducing their corrosion resistance. Hence, the UV processed samples can achieve a more stable state, thereby enhancing their corrosion resistance.

4. Conclusions

In this work, a UV treatment method was developed to enhance the corrosion resistance of BMG. Compared with Microalloying, ion implantation technology and heat treatment, UV treatment offers a highly efficient and convenient measure. The corrosion resistance of the UV processed samples was confirmed to be superior to that of the as-cast samples through electrochemical tests and micro-morphology characterization in our study. Due to UV treatment, the atoms in the inelastic regions of the BMG are more tightly packed together, resulting in a more stable amorphous structure, thus enhancing the corrosion resistance of BMG. As a result, this work provides a promising and cost-effective route to enhance the corrosion resistance of BMGs, thus broadening their engineering applications.

CRediT authorship contribution statement

Lixing Zhu: Writing – original draft, Visualization, Validation, Methodology, Investigation, Formal analysis, Data curation. Luyao Li: Validation, Methodology, Investigation, Data curation. Jinbiao Huang: Methodology, Investigation. Heting Zhang: Supervision. Wenxue Wang: Supervision. Jianyu Chen: Supervision. Junsheng Liu: Supervision. Jiang Ma: Writing – review & editing, Supervision.

Declaration of competing interest

The authors declare that they have no known competing financial interests or personal relationships that could have appeared to influence the work reported in this paper.

Data availability

Data will be made available on request.

Acknowledgements

The work was financially supported by the NSF of China (Grant No. 52122105, 52271150, 52201185, 52201186, 52371160), and the Science and Technology Innovation Commission Shenzhen (Grants No. RCJC20221008092730037, 20220804091920001) and the Research Team Cultivation Program of Shenzhen University (Grant No. 2023QNT001). The authors also thank the assistance on microscope observation received from the Electron Microscope Center of the Shenzhen University.

Supplementary materials

Supplementary material associated with this article can be found, in the online version, at doi:10.1016/j.jnoncrysol.2024.123223.

References

- [1] Y. Shi, B. Yang, P.K. Liaw, Corrosion-resistant high-entropy alloys: a review, Metals (Basel) 7 (2) (2017) 43, https://doi.org/10.3390/met7020043.
- [2] V.N. Kumar, A. Sil, Five decades spatial hazard maps of atmospheric corrosion predict the rate of deterioration of steel beams in different environments of India, Corros. Rev. 41 (1) (2023) 85–101, https://doi.org/10.1515/corrrev-2022-0028.
- [3] S. Doshvarpassand, C. Wu, X. Wang, An overview of corrosion defect characterization using active infrared thermography, Infrared Phys. Techn. 96 (2019) 366–389, https://doi.org/10.1016/j.infrared.2018.12.006.
- [4] L. Liu, Y. Li, F. Wang, Electrochemical corrosion behavior of nanocrystalline materials—A review, J. Mater. Sci. Technol. 26 (1) (2010) 1–14, https://doi.org/ 10.1016/S1005-0302(10)60001-1.
- [5] Z. Huang, X. Liang, C. Chang, J. Ma, WEDM-LS processing sophisticated and durable Zr-based metallic glass mold insert for micro structure injection of polymers, Biomed. Microdevices 21 (2019) 1–7, https://doi.org/10.1007/s10544-019-0366-0.
- [6] J. Schroers, G. Kumar, T.M. Hodges, S. Chan, T.R. Kyriakides, Bulk metallic glasses for biomedical applications, JOM 61 (2009) 21–29, https://doi.org/10.1007/ s11837-009-0128-1.
- [7] W.H. Wang, Roles of minor additions in formation and properties of bulk metallic glasses, Prog. Mater. Sci. 52 (4) (2007) 540–596, https://doi.org/10.1016/j. pmatsci.2006.07.003.
- [8] A. Inoue, Stabilization of metallic supercooled liquid and bulk amorphous alloys, Acta. Mater. 48 (1) (2000) 279–306, https://doi.org/10.1016/S1359-6454 (99) 00300-6.
- [9] C.A. Schuh, T.C. Hufnagel, U. Ramamurty, Mechanical behavior of amorphous alloys, Acta. Mater. 55 (12) (2007) 4067–4109, https://doi.org/10.1016/j. actamat.2007.01.052.
- [10] A. Greer, Y. Cheng, E. Ma, Shear bands in metallic glasses, Mat. Sci. Eng. R. 74 (4) (2013) 71–132, https://doi.org/10.1016/j.mser.2013.04.001.
- [11] W. Klement, R. Willens, P. Duwez, Non-crystalline structure in solidified gold-silicon alloys, Nature 187 (4740) (1960) 869–870, https://doi.org/10.1038/ 18786010
- [12] J. Huang, X. Yu, L. Li, W. Wang, H. Zhang, Y. Zhang, J. Zhu, J. Ma, Design of light-driven biocompatible and biodegradable microrobots containing mg-based metallic glass nanowires, ACS Nano 18 (3) (2024) 2006–2016, https://doi.org/10.1021/acsnano.3c08277.
- [13] J.J. Kruzic, Bulk metallic glasses as structural materials: a review, Adv. Eng. Mater. 18 (8) (2016) 1308–1331, https://doi.org/10.1002/adem.201600066.
- [14] W.-H. Wang, C. Dong, C. Shek, Bulk metallic glasses, Mat. Sci. Eng. R. 44 (2–3) (2004) 45–89, https://doi.org/10.1002/adma.200901053.
- (2004) 43–89, https://doi.org/10.1002/adma.200901053.
 W. Wang, Bulk metallic glasses with functional physical properties, Adv. Mater. 21 (45) (2009) 4524–4544, https://doi.org/10.1002/adma.200901053.
- [16] C. Yuan, Z. Lv, C. Pang, X. Li, R. Liu, C. Yang, J. Ma, H. Ke, W. Wang, B. Shen, Ultrasonic-assisted plastic flow in a Zr-based metallic glass, Sci. China Mater. 64 (2) (2021) 448–459, https://doi.org/10.1007/s40843-020-1411-2.
- [17] F. Sun, X. Yu, J. Fu, Y. Zhu, W. Wang, R. Sun, H. Zhang, F. Gong, J. Ma, J. Shen, High-temperature wear behavior of a Zr-based metallic glass, J. Alloy Compd. 960 (2023) 170703, https://doi.org/10.1016/j.jallcom.2023.170703.

- [18] D. Wang, S. Wang, J. Wang, Relationship between amorphous structure and corrosion behaviour in a Zr–Ni metallic glass, Corros. Sci. 59 (2012) 88–95, https://doi.org/10.1016/j.corsci.2012.02.017.
- [19] J. Schroers, Processing of bulk metallic glass, Adv. Mater. 22 (14) (2010) 1566–1597, https://doi.org/10.1002/adma.200902776.
- [20] S. González, E. Pellicer, S. Suriñach, M. Baró, J. Sort, Mechanical and corrosion behaviour of as-cast and annealed Zr60Cu20Al10Fe5Ti5 bulk metallic glass, Intermetallics 28 (2012) 149–155, https://doi.org/10.1016/j. intermet.2012.04.007
- [21] A. Gebert, U.K. Mudali, J. Eckert, L. Schultz, Electrochemical reactivity of zirconium-based bulk metallic glasses, MRS Online Proceedings Library 806 (2003) 30–40, https://doi.org/10.1557/PROC-806-MM10.2.
- [22] J.Y. Yang, J.L. Gu, S.Q. Chen, C.H. Luan, Y. Shao, K.F. Yao, Electrochemical corrosion resistance of the amorphous and crystalline Pd-based alloys in simulated seawater, Mater. Corros. 69 (11) (2018) 1509–1515, https://doi.org/10.1002/ page 201810072
- [23] C. Qin, K. Asami, T. Zhang, W. Zhang, A. Inoue, Corrosion behavior of Cu-Zr-Ti-Nb bulk glassy alloys, Mater. Trans. 44 (4) (2003) 749–753, https://doi.org/10.2320/matertrans.44.749.
- [24] H. Habazaki, H. Ukai, K. Izumiya, K. Hashimoto, Corrosion behaviour of amorphous Ni-Cr-Nb-P-B bulk alloys in 6M HCl solution, Mat. Sci. Eng. A-Struct. 318 (1-2) (2001) 77–86, https://doi.org/10.1016/S0921-5093 (01) 01324-7.
- [25] Q. Jiang, C. Qin, K. Amiya, S. Nagata, A. Inoue, R. Zheng, G. Cheng, X. Nie, J. Jiang, Enhancement of corrosion resistance in bulk metallic glass by ion implantation, Intermetallics 16 (2) (2008) 225–229, https://doi.org/10.1016/j. intermet.2007.09.009.
- [26] M. Zhou, K. Hagos, H. Huang, M. Yang, L. Ma, Improved mechanical properties and pitting corrosion resistance of Zr65Cu17. 5Fe10Al7. 5 bulk metallic glass by isothermal annealing, J. Non-Cryst. Solids 452 (2016) 50–56, https://doi.org/ 10.1016/j.jnoncrysol.2016.08.014.
- [27] R. Wang, Y. Wang, J. Yang, J. Sun, L. Xiong, Influence of heat treatment on the mechanical properties, corrosion behavior, and biocompatibility of Zr56Al16Co28 bulk metallic glass, J. Non-Cryst. Solids 411 (2015) 45–52, https://doi.org/ 10.1016/j.jnoncrysol.2014.12.018.
- [28] S. Sohrabi, J. Fu, L. Li, Y. Zhang, X. Li, F. Sun, J. Ma, W.H. Wang, Manufacturing of metallic glass components: processes, structures and properties, Prog. Mater. Sci. (2024) 101283, https://doi.org/10.1016/j.pmatsci.2024.101283.
- [29] Z. Huang, J. Fu, X. Li, W. Wen, H. Lin, Y. Lou, F. Luo, Z. Zhang, X. Liang, J. Ma, Ultrasonic-assisted rapid cold welding of bulk metallic glasses, Sci. China Mater. 65 (2021) 255–262, https://doi.org/10.1007/s40843-021-1723-6.
- [30] L. Li, X. Li, Z. Huang, J. Huang, Z. Liu, J. Fu, W. Wen, Y. Zhang, S. Huang, S. Ren, Joining of metallic glasses in liquid via ultrasonic vibrations, Nat. Commun. 14 (1) (2023) 6305, https://doi.org/10.1038/s41467-023-42014-x.
- [31] X. Li, L. Li, S. Sohrabi, J.n. Fu, Z. Li, Z. Chen, R. Sun, Y. Zhang, J. Huang, H. Zhang, Ultrasonic vibration enabled under-liquid forming of metallic glasses, Sci. Bull. 69 (2) (2024) 163–166, https://doi.org/10.1016/j.scib.2023.11.049.
- [32] Z. Chen, S. Ren, R. Zhao, J. Zhu, X. Li, H. Zhang, H. Lin, J. Zhu, S. Sohrabi, W. Ruan, Plasticity and rejuvenation of aged metallic glasses by ultrasonic vibrations, J. Mater. Sci. Technol. 181 (2024) 231–239, https://doi.org/10.1016/j. jmst.2023.09.029.
- [33] C. Yuan, Z. Lv, X. Li, C. Pang, R. Liu, C. Yang, J. Ma, W. Zhu, B. Huang, H. Ke, Ultrasonic-promoted defect activation and structural rejuvenation in a La-based metallic glass, Intermetallics 153 (2023) 107803, https://doi.org/10.1016/j. intermet.2022.107803.
- [34] X. Liang, K. Wu, J. Fu, L. Li, C. Fan, W. Wen, W. Ruan, S. Ren, Z. Zhang, J. Ma, Fabrication of amorphous and high-entropy biphasic composites using highfrequency ultrasonic vibration, J. Non-Cryst. Solids 582 (2022) 121458, https:// doi.org/10.1016/j.iponcrysol.2022.121458.
- [35] W.-X. Wen, L.-Y. Li, Z. Li, W.-Q. Ruan, S. Ren, Z.-X. Zhang, X. Liang, H. Liu, J. Ma, Ultrasonic vibration-assisted multi-scale plastic forming of high-entropy alloys in milliseconds, Rare Met. 42 (4) (2023) 1146–1153, https://doi.org/10.1007/ s15588.023.02171.2
- [36] Z. Wang, P. Chen, H. Li, B. Fang, R. Song, Z. Zheng, The intergranular corrosion susceptibility of 2024 Al alloy during re–ageing after solution treating and cold–rolling, Corros. Sci. 114 (2017) 156–168, https://doi.org/10.1016/j. corsci.2016.11.013.
- [37] T. Chieh, J. Chu, C.a. Liu, J. Wu, Corrosion of Zr52. 5Cu17. 9Ni14. 6Al10Ti5 bulk metallic glasses in aqueous solutions, Mater. Lett. 57 (20) (2003) 3022–3025, https://doi.org/10.1016/S0167-577X (02) 01424-6.
- [38] L. Liu, C. Qiu, H. Zou, K.C. Chan, The effect of the microalloying of Hf on the corrosion behavior of ZrCuNiAl bulk metallic glass, J. Alloy Compd. 399 (1–2) (2005) 144–148, https://doi.org/10.1016/j.jallcom.2005.03.016.
- [39] X. Ma, N. Zhen, J. Guo, Q. Li, C. Chang, Y. Sun, Preparation of Ni-based bulk metallic glasses with high corrosion resistance, J. Non-Cryst. Solids 443 (2016) 91–96, https://doi.org/10.1016/j.jnoncrysol.2016.04.020.
- [40] T. Xu, S. Pang, T. Zhang, Glass formation, corrosion behavior, and mechanical properties of novel Cr-rich Cr–Fe–Mo–C–B–Y bulk metallic glasses, J. Alloy Compd. 625 (2015) 318–322, https://doi.org/10.1016/j.jallcom.2014.09.166.
- [41] C. Brito, T. Vida, E. Freitas, N. Cheung, J.E. Spinelli, A. Garcia, Cellular/dendritic arrays and intermetallic phases affecting corrosion and mechanical resistances of an Al-Mg-Si alloy, J. Alloy Compd. 673 (2016) 220–230, https://doi.org/ 10.1016/j.jallcom.2016.02.161.
- [42] L. Xue, C. Liao, M. Wu, Q. Li, Z. Hu, Y. Yang, J. Liu, Improvement of mechanical properties and corrosion resistance of SLM-AlSi10Mg alloy by an eco-friendly electric pulse treatment, J. Clean. Prod. 439 (2024) 140864, https://doi.org/ 10.1016/j.jclepro.2024.140864.

- [43] S.-C. Lee, C.-M. Lee, J.-W. Yang, J.-C. Lee, Microstructural evolution of an elastostatically compressed amorphous alloy and its influence on the mechanical properties, Scripta Mater 58 (7) (2008) 591–594, https://doi.org/10.1016/j. scriptamat.2007.11.036.
- [44] X. Li, D. Wei, J. Zhang, X. Liu, Z. Li, T. Wang, Q. He, Y. Wang, J. Ma, W. Wang, Ultrasonic plasticity of metallic glass near room temperature, Appl. Mater. Today 21 (2020) 100866, https://doi.org/10.1016/j.apmt.2020.100866.
- [45] S. Sohrabi, B. Sun, M. Mahmoodan, Y. Sun, R. Gholamipour, W. Wang, Rejuvenation by compressive elasto-static loading: the role of static stress on a Zr-based metallic glass, J. Alloy Compd. 933 (2023) 167715, https://doi.org/ 10.1016/j.jallcom.2022.167715.
- [46] A. Greer, Y. Sun, Stored energy in metallic glasses due to strains within the elastic limit, PhilosMag 96 (16) (2016) 1643–1663, https://doi.org/10.1080/ 14786435.2016.1177231.
- [47] H. Zhao, F. Sun, X. Li, Y. Ding, Y. Yan, X. Tong, J. Ma, H. Ke, W. Wang, Ultrastability of metallic supercooled liquid induced by vibration, Scripta Mater 194 (2021) 113606, https://doi.org/10.1016/j.scriptamat.2020.10.048.
- [48] C. Liu, R. Maaß, Elastic fluctuations and structural heterogeneities in metallic glasses, Adv. Funct. Mater. 28 (30) (2018) 1800388, https://doi.org/10.1002/ adfm 201800388
- [49] W. Dmowski, T. Iwashita, C.-P. Chuang, J. Almer, T. Egami, Elastic heterogeneity in metallic glasses, Phys. Rev. Lett. 105 (20) (2010) 205502, https://doi.org/ 10.1103/PhysRevLett.105.205502.

- [50] W. Jiang, F. Jiang, B. Green, F. Liu, P. Liaw, H. Choo, K. Qiu, Electrochemical corrosion behavior of a Zr-based bulk-metallic glass, Appl. Phys. Lett. 91 (4) (2007), https://doi.org/10.1063/1.2762282.
- [51] R. Jindal, V. Raja, M.A. Gibson, M.J. Styles, T.J. Bastow, C. Hutchinson, Effect of annealing below the crystallization temperature on the corrosion behavior of Al–Ni–Y metallic glasses, Corros. Sci. 84 (2014) 54–65, https://doi.org/10.1016/j. corsci.2014.03.015.
- [52] F. Marzo, A. Pierna, M. Vega, Effect of irreversible structural relaxation on the electrochemical behavior of Fe78 – xSi13B9Cr (x= 3, 4, 7) amorphous alloys, J. Non-Cryst. Solids 329 (1–3) (2003) 108–114, https://doi.org/10.1016/j. inoncrysol.2003.08.022.
- [53] W. Jiang, M. Atzmon, The effect of compression and tension on shear-band structure and nanocrystallization in amorphous Al90Fe5Gd5: a high-resolution transmission electron microscopy study, Acta Mater. 51 (14) (2003) 4095–4105, https://doi.org/10.1016/S1359-6454(03)00229-5.
- [54] A.R. Yavari, A.Le Moulec, A. Inoue, N. Nishiyama, N. Lupu, E. Matsubara, W. J. Botta, G. Vaughan, M. Di Michiel, Å. Kvick, Excess free volume in metallic glasses measured by X-ray diffraction, Acta Mater. 53 (2005) 1611–1619, https://doi.org/10.1016/j.actamat.2004.12.011.
- [55] D. Gunderov, E. Boltynjuk, V. Sitdikov, G. Abrosimova, A. Churakova, A. Kilmametov, R. Valiev, Free volume measurement of severely deformed Zr62Cu22Al10Fe5Dy1 bulk metallic glass, in: Journal of Physics: Conference Series, IOP Publishing, 2018 012010, https://doi.org/10.1088/1742-6596/1134/ 1/012010.